



Two-phase modeling of sheet-flow beneath waves and its dependence on grain size and streaming



Wouter M. Kranenburg^{a,*}, Tian-Jian Hsu^b, Jan S. Ribberink^a

^a Marine and Fluvial Systems Group, Twente Water Center, University of Twente, Box 217, 7500 AE Enschede, The Netherlands

^b Center for Applied Coastal Research, Civil and Environmental Engineering, University of Delaware, Newark, DE 19716, USA

ARTICLE INFO

Article history:

Available online 27 May 2014

Keywords:

Sheet-flow
Sand transport
Turbulent wave boundary layers
Two-phase modeling

ABSTRACT

We study erosion depth and sediment fluxes for wave-induced sheet-flow, and their dependency on grain size and streaming. Hereto, we adopt a continuous two-phase model, applied before to simulate sheet-flow of medium and coarse sized sand. To make the model applicable to a wider range of sizes including fine sand, it appears necessary to adapt the turbulence closure of the model. With an adapted formulation for grain-carrier flow turbulence interaction, good reproductions of measured erosion depth of fine, medium and coarse sized sand beds are obtained. Also concentration and velocity profiles at various phases of the wave are reproduced well by the model. Comparison of sediment flux profiles from simulations for horizontally uniform oscillatory flow as in flow tunnels and for horizontally non-uniform flow as under free surface waves, shows that especially for fine sand onshore fluxes inside the sheet-flow layer increase under influence of progressive wave effects. This includes both the current-related and the wave-related contribution to the period-averaged sheet-flow sediment flux. The simulation results are consistent with trends for fine and medium sized sediment flux profiles observed from tunnel and flume experiments. This study shows that the present two-phase model is a valuable instrument for further study and parameterization of sheet-flow layer processes.

© 2014 Elsevier Ltd. All rights reserved.

1. Introduction

Under high waves sand in the near-shore zone is transported as sheet-flow. The main characteristics of this phenomenon are that bed forms are washed away and that the motion of sediment extends down to several grain diameters below the initial bed level (erosion depth). This moving layer with high concentrations of sediment (sheet-flow layer) is held responsible for the larger part of the sediment transport. Good predictions of wave-induced sediment transport rates are of utmost importance for coastal engineering work. Therefore, it is relevant to gain detailed insights in sheet-flow characteristics and transport mechanisms and to develop tools to quantify transport rates in the sheet-flow regime.

Usually, morphodynamic models make use of (semi-)empirical sediment transport formulas (e.g. [45]). These formulas are generally based on sets of experiments with a limited number of wave and bed conditions. Besides, most of these experiments have been carried out in oscillating flow tunnels, while it has become clear from recent flume experiments that free surface effects not

included in these tunnel experiments can largely affect the transport rates and underlying processes. Detailed numerical models can be helpful to investigate parameter values that have not been investigated experimentally and to improve the insight in underlying processes. Subsequent parameterization of the numerical model results can help to improve the physical basis of these transport formulas.

For these process-studies and parameterizations various types of numerical models are available. Here we mention (quasi) single phase and continuous two-phase wave boundary layer models. In single phase or suspension models, particles are, apart from the settling velocity, assumed to move with the fluid velocity, and sediment concentrations are determined from an advection–diffusion equation with a fixed-level lower boundary condition that relates the near-bed concentration or vertical sediment flux to the local shear stress through an empirical reference concentration or pick-up function. Models of this type have been very helpful to investigate the influence of e.g. the wave shape [26,47], grain size [21], stratification [10] and free surface effects [6,18,27,35,36] on boundary layer flow and/or sediment transport. Besides, they have been applied to predict bar migration [22,28]. An important lesson from these studies – in line with empirical findings of [12,43] – concerns the phase-lag behavior of fine sand: due to a small

* Corresponding author. Tel.: +31 53 4892959; fax: +31 534895377.

E-mail addresses: w.m.kranenburg@gmail.com (W.M. Kranenburg), thsu@udel.edu (T.-J. Hsu), j.s.ribberink@utwente.nl (J.S. Ribberink).

settling velocity fine sand can be stirred up during the flow motion in one direction but (partly) transported during the reverse motion. For velocity skewed oscillatory flow (modeling e.g. 2nd order Stokes waves), this can result in net offshore transport for fine sand compared to onshore transport for medium and coarse sized sand. Another lesson concerned the contribution to onshore sediment transport by ‘progressive wave streaming’, an onshore directed bottom boundary layer current under influence of vertical orbital motions in the horizontally non-uniform flow beneath progressive waves [38]. For medium sized sand, this process leads to increased onshore transport rate compared to what is found in tunnels. However, for fine sand it can even reverse the net transport direction from offshore (in oscillatory flow) to onshore (under progressive waves) [6,18,35].

Notwithstanding these valuable insights in sand transport behavior, the principle set-up of these models implicates that they cannot solve the details of the sheet-flow layer, like the fluctuating position of the bed, the shape of the flux profile up to this level and the adapted flow and sediment dynamics in the region of high sediment concentrations [18]. Alternatively, sheet-flow models have been developed based on theory for continuous two-phase flow. These models describe the motion of water and sediment from the immobile bed into the suspension layer with individual mass and momentum equations and mutual interactions between the phases. In principle, this makes it possible to simulate sediment suspension processes without empirical functions for reference concentrations or sediment pick-up and without any need to distinguish between bed load and suspended load. Examples of this type of models are [4,14,30,37,35]. Differences between the various two-phase models appear in the closures of respectively the turbulent stresses, either with mixing length, one-equation or two-equation turbulence closures, and interparticle stresses, either modeled with rheological equations like Bagnold’s expressions for the viscous and inertia regime ([5], see also [1]), or using the concept of ‘granular temperature’ from collisional granular flow theory for the energy of the particle fluctuations [32]. Next, differences are found in the modeling of the particle–fluid interaction, both on the level of momentum equations (e.g. different descriptions of the drag force, omission of the added mass force) and concerning the particle influence on the carrier flow turbulence. Two-phase models, in principle all able to deal with oscillatory flows of different shape, have been applied in e.g. process-research on the influence of the wave shape [31], and for parameterization of the vertical sediment flux [54]. So far only [55] considered progressive wave streaming and other free surface effects by including horizontal and vertical advection in fluid, sediment and closure equations. However, this two-phase model – like many others – has been validated and is applicable for medium and coarse grains only.

As discussed above, fine sand can show a transport behavior under influence of wave shape and progressive wave effects significantly different from medium and coarse sized sand. To further improve sediment transport formulas, responsible processes need to be understood and parameterized. Therefore, it is the objective of this paper to predict sheet-flow layer behavior under progressive waves for sand sizes ranging from fine to coarse (0.1–0.5 mm). Characteristics we are especially interested in are erosion depth, sheet-flow layer thickness and the vertical distribution of the (wave- and current related components of the) sediment flux. Hereby, the dependency on grain size and the influence of progressive wave effects are central questions. To study this, we adopt the two-phase model of [55] and extend its applicability to fine grains by implementing an improved formulation for the particle influence on the fluid turbulence. We thus combine the advantage of continuum two-phase models over single-phase models in predicting the entire flux profile, with both the

inclusion of progressive wave effects and the simulation of fine sand dynamics.

The set-up of the paper is as follows: Section 2 describes the background and set-up of the model. Section 3 describes the data selected for model validation. Section 4 shows validation tests on erosion depths for various grain sizes and explains why the model adaptation proposed in this study improves the model performance for fine sand. Next, Section 5 discusses a model-data comparison on time-dependent concentration profiles and time-dependent and wave-averaged velocity profiles, the latter both with and without progressive wave streaming. Subsequently, in Section 6 the model is applied to investigate trends in sediment flux profiles for fine and medium sized sand both without and with progressive wave streaming. Finally, Sections 7 and 8 respectively provide a discussion and summary of the conclusions.

2. Model formulation

2.1. Model background

The two-phase model we adopt here has been developed originally by Hsu et al. [29] for dilute sediment transport in steady and oscillatory flow. It has subsequently been extended with interparticle stress formulations to model sheet-flow of massive particles [30]. Amoudry et al. [3] have applied the model to sheet-flow of coarse and medium sized sand, meanwhile pointing at the limits for application to fine sand. The model applicability has been extended by Yu et al. [55] from horizontally uniform flow as present in oscillatory flow tunnels to horizontally non-uniform flow as present under propagating waves.

The model can be classified as a 1DV two-phase model with a two-equation (k - ε) fluid turbulence and an interparticle stress closure using the ‘granular temperature’ concept. The turbulence averaged momentum equations have been derived using Favre-averaging. In Favre-averaging, ensemble-averaging is applied to the momentum per unit mass of each phase instead of the velocity. As a result, the correlation between concentration and velocity fluctuations, commonly called turbulent suspension flux, appears in the momentum equations instead of the continuity equations [40]. The horizontal non-uniformity has been accounted for within the 1DV approach by the transformation:

$$\frac{\partial}{\partial x} = -\frac{1}{c} \frac{\partial}{\partial t} \quad (1)$$

which assumes that the waves propagate (with c the propagation velocity) without changing their form. Below, the model equations are given in the averaged and transformed form, as solved by the numerical model.

2.2. Governing equations

The continuity equations for the fluid (f) and sediment (s) phase are:

$$-\frac{1}{c} \frac{\partial(1-\phi)w^f}{\partial t} + \frac{\partial(1-\phi)w^f}{\partial z} - \frac{\partial\phi}{\partial t} = 0 \quad (2)$$

and

$$-\frac{1}{c} \frac{\partial\phi u^s}{\partial t} + \frac{\partial\phi w^s}{\partial z} + \frac{\partial\phi}{\partial t} = 0 \quad (3)$$

with ϕ the volumetric concentration of sediment and u and w the (Favre-averaged) velocity components in horizontal (x) respectively vertical (z) direction. The momentum equations of the fluid phase in the x - and z -directions can respectively be written as:

$$\left(1 - \frac{u^f}{c}\right) \frac{\partial u^f}{\partial t} + w^f \frac{\partial u^f}{\partial z} = -\frac{1}{\rho^f} \frac{\partial P^f}{\partial x} + \frac{1}{\rho^f(1-\phi)} \frac{\partial \tau_{xz}^f}{\partial z} - \frac{\beta\phi}{\rho^f(1-\phi)} (u^f - u^s) - \frac{\beta v_{ft}}{c\rho^f(1-\phi)\sigma_c} \frac{\partial \phi}{\partial t} \quad (4)$$

and

$$\frac{1}{\rho^f} \frac{\partial P^f}{\partial z} = -\left(1 - \frac{u^f}{c}\right) \frac{\partial w^f}{\partial t} - w^f \frac{\partial w^f}{\partial z} + \frac{1}{\rho^f(1-\phi)} \frac{\partial \tau_{zz}^f}{\partial z} + g - \frac{\beta\phi}{\rho^f(1-\phi)} (w^f - w^s) + \frac{\beta v_{ft}}{\rho^f(1-\phi)\sigma_c} \frac{\partial \phi}{\partial z} \quad (5)$$

with P^f the fluid pressure, g the gravitational acceleration, ρ^f the fluid density, and τ_{xz}^f and τ_{zz}^f the shear and normal stresses of the fluid phase. The fluid stresses include both the viscous and turbulent stresses, the latter modeled using the Boussinesq hypothesis. The last two terms of both equations originate from interface momentum transfer by drag. Hereby, the second term appears as a result of the ensemble-averaging: parallel to the Boussinesq hypothesis, the correlation between concentration and velocity fluctuations is modeled using a gradient transport [40], with v_{ft} the eddy viscosity and σ_c the Prandtl–Schmidt number (see [34] for an elaboration hereof). The closure for v_{ft} is discussed later. Drag parameter β [kg/m³/s] is a function of particle diameter d , fluid density ρ^f , relative velocity magnitude $U_r = |\vec{u}^f - \vec{u}^s|$ and particle Reynolds number $Re_p = U_r d / \nu_f$:

$$\beta = \frac{\rho^f U_r}{d} \left(\frac{18}{Re_p} + 0.3 \right) \frac{1}{(1-\phi)^n} \quad (6)$$

A concentration dependent correction factor $(1-\phi)^{-n}$ is added to account for increased drag under influence of surrounding particles [44]. Herein, coefficient n depends on ϕ and Re_p and is computed following [17] (p. 200).

The fluid motion is driven by the horizontal pressure gradient. In the earlier versions of the model, a periodic pressure gradient was computed from a prescribed periodic horizontal velocity in the free-stream U_∞^f using $\partial P^f / \partial x = -\rho^f (1 - U_\infty^f / c) \partial U_\infty^f / \partial t$. Additionally, it is now also possible to force the model to match any prescribed velocity signal $u^f(t)$ at $z = z_{\text{match}}$, where $u^f(t)$ consists of both the periodic and mean velocity component and z_{match} can be either outside or within the wave boundary layer. This adaptation has been realized to facilitate model-data comparison, also for experiments with velocity profile measurement that do not extend up to the free stream. In this procedure the pressure gradient is determined iteratively considering also the momentum exchange by shear and vertical advection around $z = z_{\text{match}}$, and includes the effects of the condition that the time-mean flow rate in a closed facility must be zero. See [34] for details and accuracy tests. In both cases, the vertical fluid velocity is solved from the fluid continuity equation, while the fluid momentum equation in z -direction is used to determine the vertical pressure gradient, needed to solve the sediment motion (see Eq. (8)).

The momentum equations of sediment phase in the x - and z -directions are respectively

$$\left(1 - \frac{u^s}{c}\right) \frac{\partial \phi u^s}{\partial t} - \frac{\phi u^s}{c} \frac{\partial u^s}{\partial t} + \frac{\partial \phi u^s w^s}{\partial z} = -\frac{\phi}{\rho^s} \frac{\partial P^f}{\partial x} + \frac{1}{\rho^s} \frac{\partial \tau_{xz}^s}{\partial z} + \frac{\beta\phi}{\rho^s} (u^f - u^s) + \frac{\beta v_{ft}}{c\rho^s\sigma_c} \frac{\partial \phi}{\partial t} \quad (7)$$

and

$$\left(1 - \frac{u^s}{c}\right) \frac{\partial \phi w^s}{\partial t} - \frac{\phi w^s}{c} \frac{\partial u^s}{\partial t} + \frac{\partial \phi w^s w^s}{\partial z} = -\frac{\phi}{\rho^s} \frac{\partial P^f}{\partial z} + \phi g + \frac{1}{\rho^s} \frac{\partial \tau_{zz}^s}{\partial z} + \frac{\beta\phi}{\rho^s} (w^f - w^s) - \frac{\beta v_{ft}}{\rho^s\sigma_c} \frac{\partial \phi}{\partial z} \quad (8)$$

with ρ^s the sediment density and τ_{xz}^s and τ_{zz}^s the shear and normal sediment stresses, discussed later.

2.3. Closures for the fluid and particle stresses

The fluid stresses are modeled using the Boussinesq hypothesis, with the eddy viscosity defined as:

$$v_{ft} = C_\mu \frac{(1-\phi)k_f^2}{\varepsilon_f} \quad (9)$$

The two-equation turbulence model to compute the fluid phase turbulent kinetic energy k_f and the turbulent dissipation rate ε_f is described with the transport equations:

$$\left(1 - \frac{u^f}{c}\right) \frac{\partial k_f}{\partial t} + w^f \frac{\partial k_f}{\partial z} = \frac{1}{\rho^f(1-\phi)} \left(\tau_{xz}^{ft} \frac{\partial u^f}{\partial z} + \tau_{zz}^{ft} \frac{\partial w^f}{\partial z} \right) + \frac{1}{(1-\phi)} \frac{\partial}{\partial z} \left[\left(v + \frac{v_{ft}}{\sigma_k} \right) \frac{\partial (1-\phi)k_f}{\partial z} \right] - \varepsilon_f + \frac{(s-1)g v_{ft}}{(1-\phi)\sigma_c} \frac{\partial \phi}{\partial z} - \frac{1}{\rho^f(1-\phi)} \phi \beta (1-\alpha) 2k_f \quad (10)$$

and

$$\left(1 - \frac{u^f}{c}\right) \frac{\partial \varepsilon_f}{\partial t} + w^f \frac{\partial \varepsilon_f}{\partial z} = \frac{C_{\varepsilon 1} \varepsilon_f}{k_f} \frac{1}{\rho^f(1-\phi)} \left(\tau_{xz}^{ft} \frac{\partial u^f}{\partial z} + \tau_{zz}^{ft} \frac{\partial w^f}{\partial z} \right) + \frac{1}{(1-\phi)} \frac{\partial}{\partial z} \left[\left(v + \frac{v_{ft}}{\sigma_\varepsilon} \right) \frac{\partial (1-\phi)\varepsilon_f}{\partial z} \right] - \frac{C_{\varepsilon 2} \varepsilon_f}{k_f} \varepsilon_f + \frac{C_{\varepsilon 3} \varepsilon_f (s-1)g v_{ft}}{k_f (1-\phi)\sigma_c} \frac{\partial \phi}{\partial z} - C_{\varepsilon 3} \frac{1}{\rho^f(1-\phi)} \phi \beta (1-\alpha) 2\varepsilon_f \quad (11)$$

with specific density $s = \rho^s / \rho^f$. The first three terms on the right-hand side of the transport equations describe respectively production, diffusion and dissipation. The last two terms describe modifications to the standard k - ε model due to interactions between the sediment and the fluid flow turbulence through drag [11,15,16]. Because of their importance to this study, the background of these terms is briefly summarized in Appendix A.1. The fourth term can be seen as the buoyancy production/dissipation due to sediment-induced density stratification. The fifth term is a damping term that models the drag-effect on the carrier flow turbulence of sediment particles that cannot completely follow the turbulent fluid velocity fluctuations due to particle inertia. In this term, α is a parameter to characterize the degree the particles follow the fluid fluctuation. Or more precise: α is the ratio between the ensemble averaged correlation of fluid and particle velocity fluctuations and the ensemble averaged correlation of the fluid velocity fluctuation with itself. α has a value between 0 and 1, where $\alpha = 1$ denotes completely passive particles, yielding no drag-induced turbulence damping.

The question how to include the effect of sediment on the carrier flow turbulence is answered in different ways in literature. Some authors propose modifications of the turbulence model coefficients. Amoudry et al. [3] e.g. adopted a particle concentration and inertia dependent $C_{\varepsilon 2}$. Following [55], we apply the model with the standard (clear fluid) values for C_μ , $C_{\varepsilon 1}$, $C_{\varepsilon 2}$, σ_k and σ_ε (see

Table 1
Coefficients turbulence model.

Symbol	Meaning	Value
σ_c	Prandtl–Schmidt number	0.7
$\sigma_k, \sigma_\varepsilon, C_\mu, C_{\varepsilon 1}, C_{\varepsilon 2}$	Coefficients in turbulence model	1.0; 1.3; 0.09; 1.44; 1.92

Table 1), and strive after modeling the sediment effect entirely through the description of the physical interaction mechanisms of buoyancy and drag and parameters therein. The sediment related $C_{\varepsilon 3} = 1.2$, based on [16]. Fluctuation correlation coefficient α is expressed as a function of the parameters T_t and T_p , respectively

$$T_t = \frac{1}{6} \frac{k_f}{\varepsilon_f} \quad \text{and} \quad T_p = \frac{\rho_s}{\beta} \quad (12)$$

which denote the characteristic time-scale of the fluid turbulence and the particle response time. The latter is a measure of the time to accelerate a single particle from rest to the velocity of the surrounding fluid by drag. A relative small T_p yields a large correlation between particle and fluid fluctuation ($\alpha \rightarrow 1$). Based on [48], Yu et al. [55] applied

$$\alpha = \frac{1}{(1 + T_p/T_t)} \quad (13)$$

In this study, we propose

$$\alpha = \frac{1}{1 + c_1(T_p/T_t)^2} \quad (14)$$

with coefficient c_1 set to 1.2 after calibration. This model adaptation is based on considerations on limit behavior, a new analytical derivation and validation tests, and, though small, turns out to be essential to extend the model's applicability to fine sand. We return to this issue in Section 4. Finally, following examples for density stratified flow, the buoyancy term in the epsilon equation is switched off for stable stratifications (e.g. [46]).

The sediment (particle) stresses result from interparticle interactions. The way particles interact differs throughout the water column. For the closure of the sediment stresses, various regions have been discerned [20,56], for which different descriptions of the particle stress are needed. High in the water column, the concentration of suspended sediment is very low (dilute region). In that region, particle–particle interactions can be neglected and the particle suspension is supported by turbulent mixing only. In the region below, the particles move more or less independent of each other, but occasionally transfer momentum through binary collisions (collisional region). Between the immobile bed and the collisional region, a transition region is present where the grains are able to move slowly, but stay in contact with several other grains (quasi-static regime of enduring contact). This is typically the case when the sediment volume concentration ϕ is between the random close-packing and random loose-packing value, i.e. between 0.635 and 0.57. In this regime, there is transfer of momentum through friction and normal stress – like in a solid – while the material is moving like fluid though with low mobility. See Fig. 1 for a schematization.

In the collisional regime, the behavior of the grains is modeled using the kinetic theory of granular flow. This theory is based on kinetic theory of gases describing the behavior of molecules, extended to account for slightly inelastic collisions and interstitial fluid (e.g. [33]). Key elements are a constitutive relation of particle stresses for moving identical, frictionless, slightly inelastic, colliding spherical particles and a transport equation for the energy of the particle velocity fluctuations or ‘granular temperature’ Θ , respectively

$$\tau_{ij}^s = \left(-p_s + \xi_s \frac{\partial u_k^s}{\partial x_k} \right) \delta_{ij} + \mu_s \left(\frac{\partial u_i^s}{\partial x_j} + \frac{\partial u_j^s}{\partial x_i} \right) \quad (15)$$

and

$$\begin{aligned} \rho^s \left[\left(1 - \frac{u^s}{c} \right) \frac{\partial \phi \Theta}{\partial t} - \frac{\phi \Theta}{c} \frac{\partial u^s}{\partial t} + \frac{\partial \phi \Theta w^s}{\partial z} \right] \\ = \tau_{xz}^s \frac{\partial u^s}{\partial z} + \tau_{zz}^s \frac{\partial w^s}{\partial z} - \frac{\partial Q}{\partial z} - \gamma + 2\beta\phi(\alpha k_f - \Theta) \end{aligned} \quad (16)$$

In the latter equation, the first two right-hand side terms represent production of particle velocity fluctuations by shear. Q represents the flux of the fluctuation energy and γ the dissipation from inelastic collisions. The fifth term describes the effect of fluid–sediment interaction, with $2\beta\phi\alpha k_f$ a source due to fluid turbulence and $-2\beta\phi\Theta$ a sink due to drag. The symbols p_s , ξ_s and μ_s in the first equation denote granular pressure, bulk viscosity and shear viscosity. Note that Q , γ , p_s , ξ_s and μ_s itself are also functions of the volumetric sediment concentration ϕ , the granular temperature Θ and properties of the sediment. In the region of enduring contact, the main assumption of the kinetic theory (binary collisions) is no longer appropriate. Therefore additional closures are adopted in that regime introducing increased shear viscosity to account for the effect of frictional bonds and extra normal stress due to packed identical spheres in Hertzian contact. See [30] for a complete description of the closures, parameters and boundary conditions.

2.4. Solution method

A key feature of the present two-phase model is that the flow field is resolved from within the immobile bed (including the porous bed) to the free stream: the bottom boundary conditions for the fluid phase variables (homogeneous Dirichlet conditions for u^f and w^f and standard equilibrium conditions for k and ε) are applied at the bottom of the computational domain, and fluid velocity and turbulence, though small, can be non-zero within the immobile bed. At the top, homogeneous Neumann conditions are applied for u^f , k and ε . The instantaneous location of the immobile bed level is determined by a Coulomb failure criterion and is subsequently used as bottom boundary for the particle phase. At en below that level the particle velocities u^s and w^s are set to zero. The equations are solved numerically using a grid size that is fine and uniform in the lower part of the domain (typically $\Delta z = 0.3$ mm) and gradually increases in the upper part. The time integration is carried out using a predictor corrector method with all equations solved consecutively within every step. Hereby, time step Δt is dynamically adapted to both guarantee stability and limit the computational time. Usually 25 wave periods are simulated to ensure convergence of the (wave-averaged) results.

3. Data

To test the model for both a range of grain sizes and progressive wave effects, two data sets have been selected, referred to as ODO and SCH. Set ODO originates from sheet-flow experiments in the Aberdeen Oscillatory Flow Tunnel (AOFT) [42,43]. It contains detailed measurements of the sediment concentration $c(z,t)$ throughout the sheet-flow layer obtained from Concentration Conductivity Measurements (CCM). Both sinusoidal and velocity-skewed oscillatory flows were generated both with varying period and energy, and sand beds of various compositions were investigated. This included beds of well-sorted fine, medium and coarse sized sediment (median grain size d_{50} respectively 0.13, 0.27 and 0.46 mm) and mixtures hereof. During the mixed-sediment experiments, an Ultrasonic Velocity Profiler (UVP) was present with which detailed information has been obtained on the horizontal velocity $u(z,t)$ inside the oscillating boundary layer. Set SCH results from full scale wave flume experiments in the Hannover Large Wave Flume (GWK) [49]. Regular velocity-skewed waves were generated for varying wave periods T and wave heights H and sent over a horizontal sand bed with a water depth $h = 3.5$ m above it. Set SCH contains two series, with sand beds with a median grain size d_{50} of 0.245 and 0.138 mm respectively. During both series, both CCM and UVP were applied – among other instrument – providing

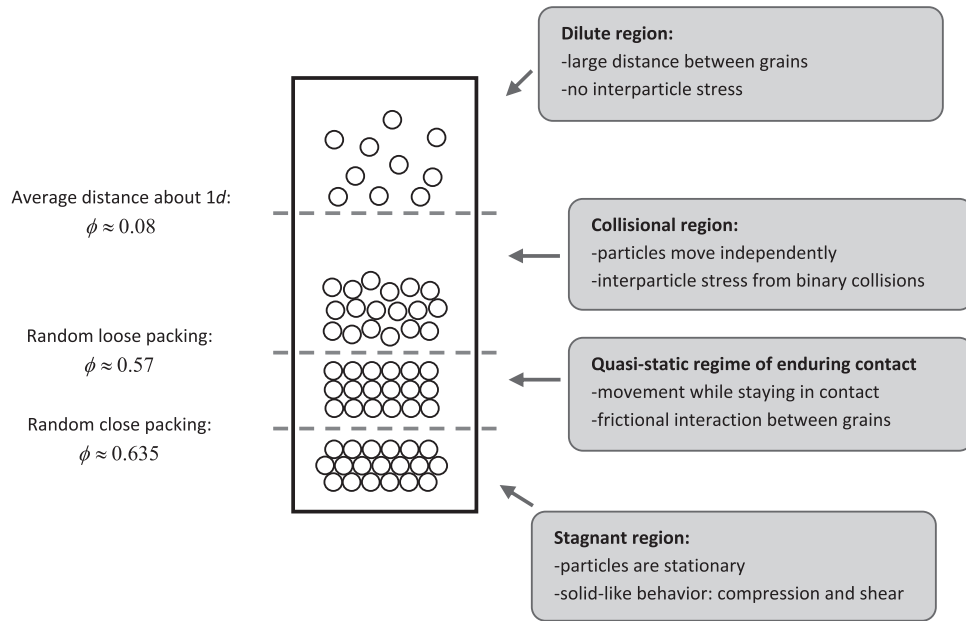


Fig. 1. Schematization of vertical regions.

concentration measurements and, for the first time, detailed information on boundary layer velocities under full scale progressive waves over a mobile bed. For both sets, averaged transport rates have been derived for each condition from bottom profile measurements with Echosounders.

Because of the range of grain sizes, set ODO is most suitable to validate grain-size dependent model behavior for erosion depth and concentration profiles. The UVP-measurements of set SCH provide unique material to validate the model's ability to predict progressive wave effects on the flow, including streaming. In principle, vertical profiles of the horizontal sediment flux can be obtained by combining the (UVP-)velocity and (CCM-)concentration measurements. However, obtaining flux profiles is not always straightforward: the flux profiles for set ODO as given by O'Donoghue and Wright [43] have been determined using the velocity information from the mixed sand tests under the assumption that these velocities are representative for the various bed conditions. The distinct results of Schretlen [49] for flow above fine and medium sized sand show that this assumption is not appropriate, especially concerning the mean current and thus the current related flux. For set SCH, quantification of the fluxes is complicated by uncertainty concerning the z -level of the measured concentrations and not well-understood deviations of the observed medium sized sand concentration profiles in some tests compared to earlier experiments for medium sized sand under velocity-skewed waves by Dohmen-Janssen and Hanes [13]. For these reasons, the primary

model validation will focus on erosion depth and concentration measurements from set ODO, while streaming profile predictions will be tested with set SCH. An overview of selected cases and characteristic parameter values is given in Table 2.

4. Model-data comparison on erosion depths

4.1. Grain size dependent erosion behavior

Fig. 2(b) shows time-series of the erosion depth δ_e of sand beds of well-sorted fine, medium and coarse sized sand under velocity-skewed oscillatory flow (condition FA7515, MA7515 and CA7515 of set ODO). Fig. 2(c) and (d) show simulation results for the erosion depth from respectively the original and the adapted model, with the new α -function proposed in this study. In all simulations the modeled flow velocity is forced to match the UVP-measured horizontal velocity at $z_{\text{match}} = 49$ mm above the original still bed level, shown in panel (a) (measurements above mixed sand bed, X1A7515). From the results, the position of the lowest model grid point with non-zero sediment velocity is taken as the erosion depth.

The original model results in Fig. 2(c) show erosion of the sand beds beneath both the onshore and offshore phase of the oscillatory flow, and a reduction of δ_e during flow reversal. This is a correct reproduction of the experimentally observed

Table 2
Overview of selected validation cases and characteristic parameter values.^a

Name	Set	T [s]	d_{50} [mm]	z_{match} [mm]	U_0 [m/s]	$u_{\text{on,red}}$ [m/s]	$u_{\text{off,red}}$ [m/s]	u_{rms} [m/s]	A [m]	RE [-]	A/k_N [-]	θ_{max} [-]	Ψ [-]	$q_{s,\text{meas}}$ [10^{-6} m ² /s]	$q_{s,\text{comp}}$ [10^{-6} m ² /s]
CA7515	ODO	7.5	0.46	49	-0.030	1.36	-0.93	0.81	1.37	1.6E6	1.5E3	1.1	1.8E2	34	17
MA7515	ODO	7.5	0.27	49	-0.030	1.36	-0.93	0.81	1.37	1.6E6	2.5E3	1.7	3.0E2	36	19
FA7515	ODO	7.5	0.13	49	-0.030	1.36	-0.93	0.81	1.37	1.6E6	5.3E3	3.0	6.3E2	-88	-20
1575medi	SCH	7.5	0.245	40	-0.063	1.42	-0.59	0.68	1.15	1.1E6	2.3E3	2.1	2.3E2	42	33
1575fine	SCH	7.5	0.138	40	-0.109	1.67	-0.78	0.80	1.36	1.5E6	4.9E3	4.3	5.8E2	70	104

^a Parameter definitions: T : wave/oscillation period; d_{50} : median grain size; U_0 : wave averaged horizontal velocity; u_{red} : reduced velocity signal, i.e. the oscillating part of the velocity only ($u(t) - U_0$); $u_{\text{on,red}}$ and $u_{\text{off,red}}$: maximum onshore respectively offshore value of u_{red} ; u_{rms} : root mean square of the complete velocity signal; water particle semi-excision $A = \sqrt{2}u_{\text{rms}}\omega^{-1}$; flow Reynolds number $Re = A\sqrt{2}u_{\text{rms}}\nu^{-1}$; relative roughness parameter A/k_N with indicative roughness height $k_N = 2d_{50}$; Shields number $\theta_{\text{max}} = \frac{1}{2}f_w u_{\text{on,red}}^2 (\Delta g d_{50})^{-1}$ with $f_w = \exp(5.213A/k_N^{0.194} - 5.977)$ [57]; mobility parameter $\Psi = 2u_{\text{rms}}^2 (\Delta g d_{50})^{-1}$.

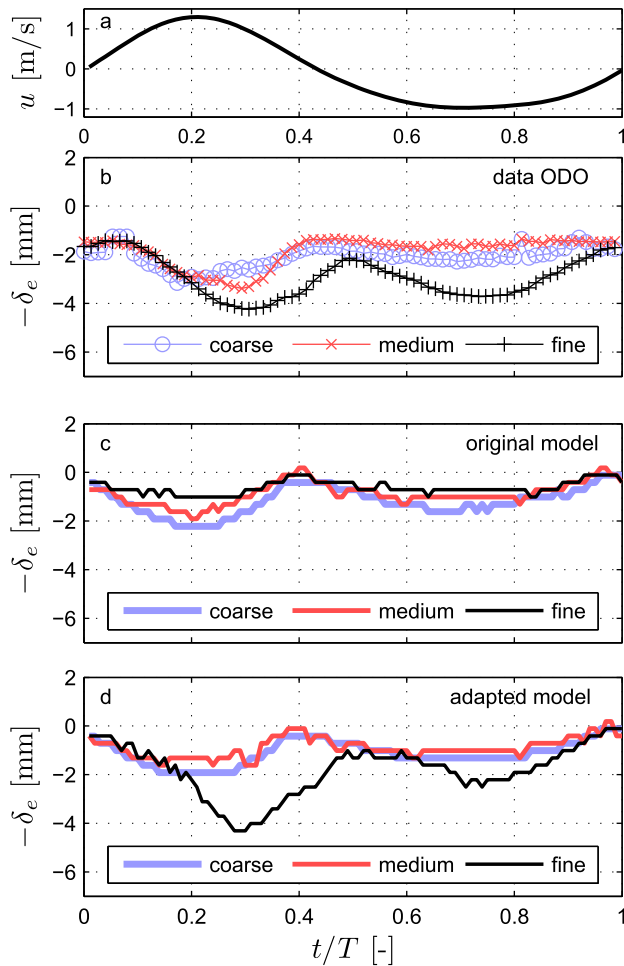


Fig. 2. Erosion depth δ_e for sand beds of coarse ($d_{50} = 0.46$ mm), medium (0.27 mm) and fine (0.13 mm) sized sand under velocity skewed oscillatory flow. Panel (a) horizontal fluid velocity at $z = z_{\text{match}}$; (b) experimental results; (c) and (d) simulation results. Conditions: CA7515, MA7515 and FA7515, see Table 2.

sheet-flow layer behavior (panel b). However, the model results show fast and relatively deep erosion for the coarse grains and only little erosion for the fine grains, which is contradictory to what we intuitively expect for varying grain size and especially for fine grains clearly not in line with the experimental results. Contrary to the original model, the results of the adapted model (d) correctly show the largest erosion depths for fine sand beds. Next, the minimum erosion depth for coarse and medium grains coincides with the reversal of the flow (see panel a), while this minimum occurs later and is deeper for fine sand. Also these features of the new model results are consistent with the data. They reflect the typical phase-lag behavior: the slow settling of fine sediment causes large amounts of sand still in suspension at the moment of flow reversal, preventing the bed level from returning to the original still bed level. Although this process might still be slightly underestimated by the model – indicated by e.g. the larger difference between the fine sand erosion maxima beneath the two velocity peaks in the model results compared to the data – we can conclude that the adapted model shows a significantly improved grain size dependent erosion behavior, which is of utmost importance to extend the model’s applicability to fine sand.

4.2. The role of fluctuation correlation coefficient α

The relevant difference between the original and adapted model concerns the fluctuation coefficient α in the drag related grain

influence on the flow turbulence. Here we discuss why we have focused on this closure to improve the pick-up behavior for fine sand and explain why the proposed formulation leads to improved results.

Sediment pick-up is related to bed shear stress, unsatisfactory pick-up behavior is therefore probably related to inaccurate (time dependent) bed shear stress. The total bed shear stress is influenced both by turbulent and intergranular stresses, with increasing importance of the first for decreasing grain size. The original model [30] has been validated on coarse grains, from which can be concluded that the intergranular stress formulations are satisfactory. Therefore, the first sub-model to be reconsidered to improve the grain-size dependent model behavior is the turbulence closure (see also [3]). Besides, the modeling of concentration effects on the carrier flow turbulence is subject of discussion in literature (e.g. [50]).

The modeled physical mechanisms of grain-turbulence interaction are buoyancy and drag. They appear in the k - ε turbulence model in the fourth and fifth RHS-term in Eqs. (10) and (11). For coarse grains, the grain inertia is relatively large (large Stokes number) while the concentration of suspended sediment will be relatively small, causing drag to be the most important interaction mechanism. Very fine particles will move easily with the flow and yield steeper concentration profiles, making buoyancy the normative mechanism. The focus on the drag term is based on sensitivity tests in the domain of our interest ($d_{50} \approx 0.1$ – 0.5 mm, $T \approx 2$ – 10 s and U_{∞}^f is order 1 m/s). For case FA7515 of set ODO e.g. tests with a 50% reduced drag-induced damping term yielded a drastic increase of the bed erosion, while effects were nearly absent for such a reduction of the buoyancy term. So for fine sand cases turbulent stresses are indeed increasingly important over intergranular stresses for sediment pick-up, while drag is still dominant over buoyancy for damping of near-bed turbulence.

Within the drag term, relevant model parameters are α , β , n and C_{e3} . The reason to focus on fluctuation coefficient α is that the α -function of Eq. (13) can be questioned based on the following theoretical consideration: Small particles will completely follow the fluid motion, while large particles are hardly accelerated by a velocity difference. Therefore any function for α should be 1 for infinitesimal small T_p/T_t and approach zero for infinitively large T_p/T_t . This is true for the original α -function from Eq. (13). However, it may also be expected that no effect of drag on turbulence is present for particles perfectly following the fluid fluctuation. This is not true when applying this function. This can be seen after substituting the expression $\beta = \rho_s/T_p$ from Eq. (12) into the drag terms of the turbulence model, showing that the damping effect of drag on k and ε is proportional to $(1 - \alpha)/T_p$. For infinitesimal small T_p/T_t and α from Eq. (13), $(1 - \alpha)/T_p$ does not approach zero, but $1/T_t$ (see Fig. 3). As a result, in the concentrated region near the bed the damping term may become very large for small T_p , strongly suppressing the near bed turbulent kinetic energy and stresses, resulting in under-predicted erosion of fine sand beds.

An alternative is available from literature: [9,11] proposed an exponential function:

$$\alpha = \exp(-BT_p/T_t) \quad (17)$$

applied successfully in modeling a turbulent jet with suspended particles, with B a calibrated coefficient of about 0.08. For this function (given $B < 1$), the behavior of $(1 - \alpha)/T_p$ for small T_p/T_t already improves. Consistently, implementation of this function within the present two-phase model also led to improved erosion behavior for fine sand (see [34]). However, its limit $(1 - \alpha)/T_p = B/T_t$ still yields grain effects on turbulence for infinitesimal small T_p/T_t .

This is not the case for the α -function of Eq. (14) proposed in this study. This newly proposed function not only fulfills the limit requirements (see Fig. 3), but is also provided with a theoretical

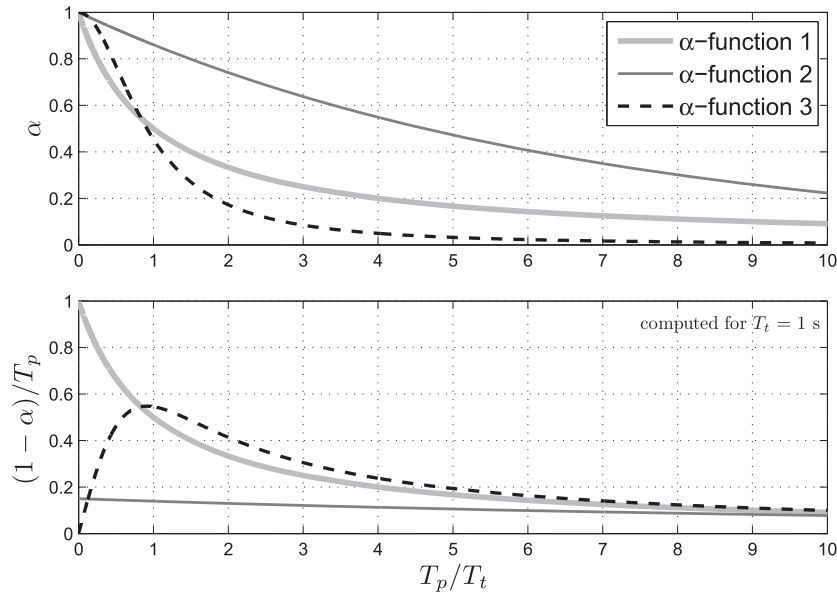


Fig. 3. Particle–fluid fluctuation correlation coefficient α (upper panel) and the accompanying damping proportionality $(1 - \alpha)/T_p$ (lower panel) as function of the relative particle response time T_p/T_t . α -Function 1: Eq. (13), the original model formulation; α -function 2: Eq. (17), an alternative from literature; α -function 3: Eq. (14), the new formulation proposed in this study. Settings: $B = 0.15$ (α -function 2); $c_1 = 1.2$ (α -function 3). Computations with $T_t = 1.0$ s.

basis. This is shown in Appendix A.2 where we derive this α -function from the fluid and particle momentum equations through transfer functions.

We can thus explain the improved results of the adapted model shown in Fig. 2 from a reduction of drag-induced turbulence damping, especially for simulations with fine grains: For identical T_b , a smaller grain size results in a smaller T_p/T_t (see Eqs. (12) and (6)). For smaller T_p/T_t , the newly proposed α -function shows less damping effect, i.e. $(1 - \alpha)/T_p$ is smaller than for the original function (see Fig. 3), resulting in more t.k.e. and more erosion. Note that estimation of the effect of changes in the turbulence model is complicated by the fact that T_t actually varies strongly with position and time in the strongly oscillating flows investigated here (compare [39]), and is itself also influenced by the drag effect.

5. Model-data comparison on concentration and velocity

5.1. Time-dependent concentration profiles for medium and fine sized sand

Further model-data comparison comprises a validation on time-dependent concentration profiles. Figs. 4 and 5 compare measured and computed profiles at various phases of a velocity skewed oscillatory flow for respectively medium and fine sized sand (condition MA7515 and FA7515 of set ODO). In the figures, phase $t/T = 0.0$ marks the beginning of onshore flow in the free stream, compare Fig. 2(a).

We conclude from the figures that, both for medium and fine sized sand, the model is able to reproduce the concentration profiles rather well: Firstly, the vertical position of the toe of the concentration profile, where $\phi = 0.6$, is followed reasonably well by the model. This result is in line with Fig. 2(d) for the erosion depth δ_e . Next, the model results show a decreasing ϕ beneath the original still bed level and an increasing ϕ above during increasing (absolute) flow velocities, which is also consistent with the data and reflects typical sheet-flow layer behavior. A closer look to the profile shapes shows that the best model-data agreement is found for medium sized sand, in particular during offshore flow (i.e. negative velocities, $0.42 < t/T < 1.0$). In some other profiles

(e.g. FA7515, $t/T = 0.21$), the simulation results show a large vertical concentration gradient just above the instantaneous erosion depth and a smaller concentration gradient at higher levels, while the data show a more linear profile. This could point at fine sand being stirred up too much after mobilization. At $t/T = 0.44$, the fine sand concentration profile is nearly horizontal, which could point at a too strong collapse of the profile during flow reversal. This is in line with the slight underestimation of the erosion depth during offshore flow mentioned before. The profile shape is determined by the balance between mixing and falling, highly related to the turbulence stresses. Although turbulence measurements are not available, a further check of the turbulence model could be possible from model-data comparison on (ensemble-averaged) velocity profiles, shown next.

5.2. Time-dependent and wave-averaged velocity profiles

Fig. 6 shows vertical profiles of horizontal velocity from the bed to the free stream at various phases of the flow for condition FA7515 of set ODO. Firstly, we observe that the course of the velocity profile from the bed to the free stream is generally followed well by the model. This includes the phase lead of the near-bed velocity over the free stream (most clear for $t/T = 0.0$ and 0.44), and the location in the upper part of the profile above which velocity shear is nearly absent. The latter means that in general the model is well capable to predict the boundary layer thickness, and thus the turbulence intensity. Model-data differences are the largest for $t/T = 0.0$ and 0.08 , i.e. around the off- to onshore flow reversal and subsequent acceleration. Here (and to a lesser extend during on- to offshore flow reversal) the simulated profiles show a rather constant velocity gradients in the lowest part of the domain. These features point at an underestimation of the vertical momentum transfer in this area, which, like earlier discussed erosion and concentration observations, can probably be explained by underestimated turbulence intensities near the bed during flow reversal.

To check the model's ability to deal with the various streaming mechanism, Fig. 7 shows a model-data comparison on wave averaged flow profiles for both tunnel (ODO) and flume (SCH) experiments, the latter with beds of both fine and medium sized sand.

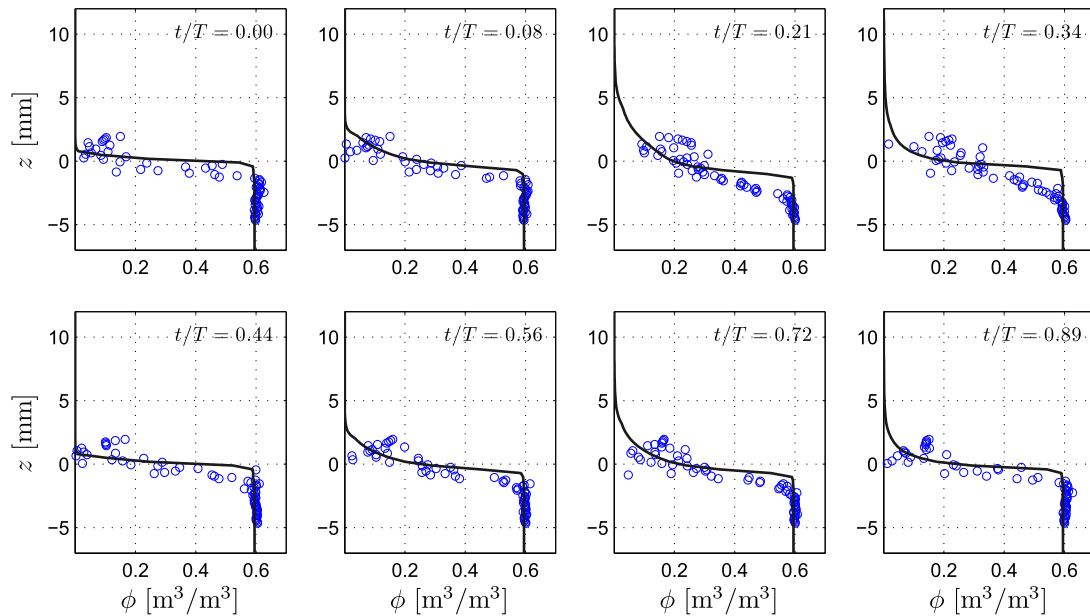


Fig. 4. Comparison of measured (circles) and computed (line) sediment concentrations at various phases of the flow for condition MA7515.

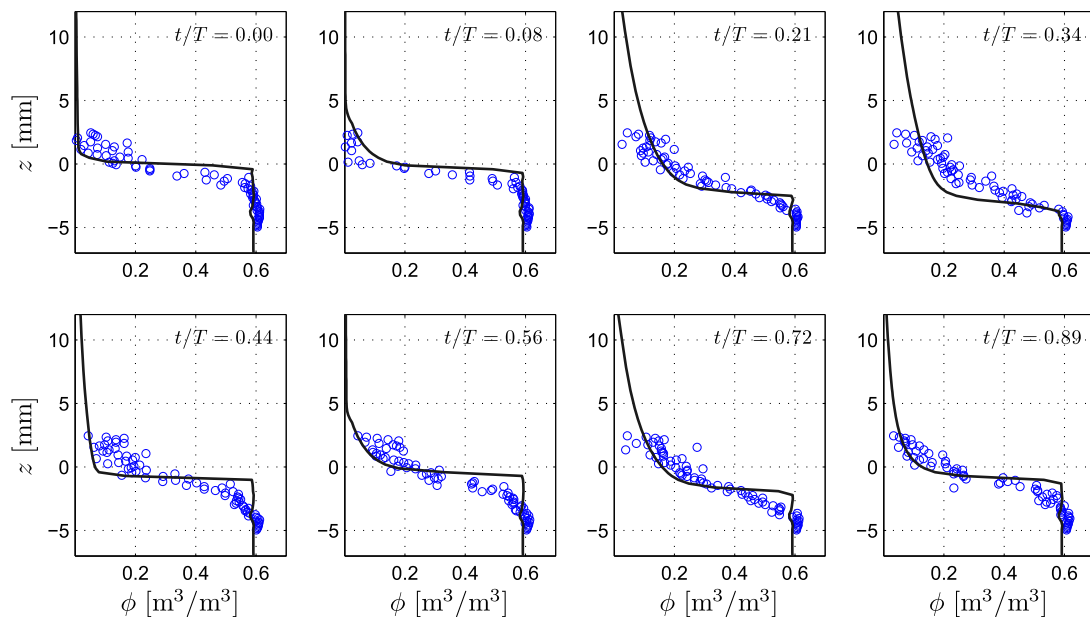


Fig. 5. Comparison of measured (circles) and computed (line) sediment concentrations at various phases of the flow for condition FA7515.

Most important observation is that for all conditions the model clearly produces the onshore mean current beneath the original still bed level, which results from differences in erosion depth between on- and offshore flow. The reproduction of this feature typical for sheet-flow under velocity skewed oscillations/waves is an important improvement compared with earlier streaming profile predictions with a single-phase/suspension model [35]. Next, for all three cases both model and data show a strong velocity gradient and an offshore current just above the original bed level. This phenomenon is explained from differences in turbulence intensity between on- and offshore flow beneath the velocity-skewed waves (wave shape streaming) [36,52]. We conclude from the results that, saving a slight underestimation for condition 1575medi, this

turbulence asymmetry is generally reproduced correctly. Finally, note the local minimum around $z = 20$ mm for the flume case data and the model results in panel b. This feature is explained from the contribution of progressive wave streaming. We therefore conclude that this typical progressive wave effect is also reproduced correctly. The importance to account for these effects is underlined by an additional simulation for case 1575fine neglecting them (dashed line).

5.3. Evaluation

The model reproduces a number of important experimentally observed sheet-flow and boundary layer characteristics. This

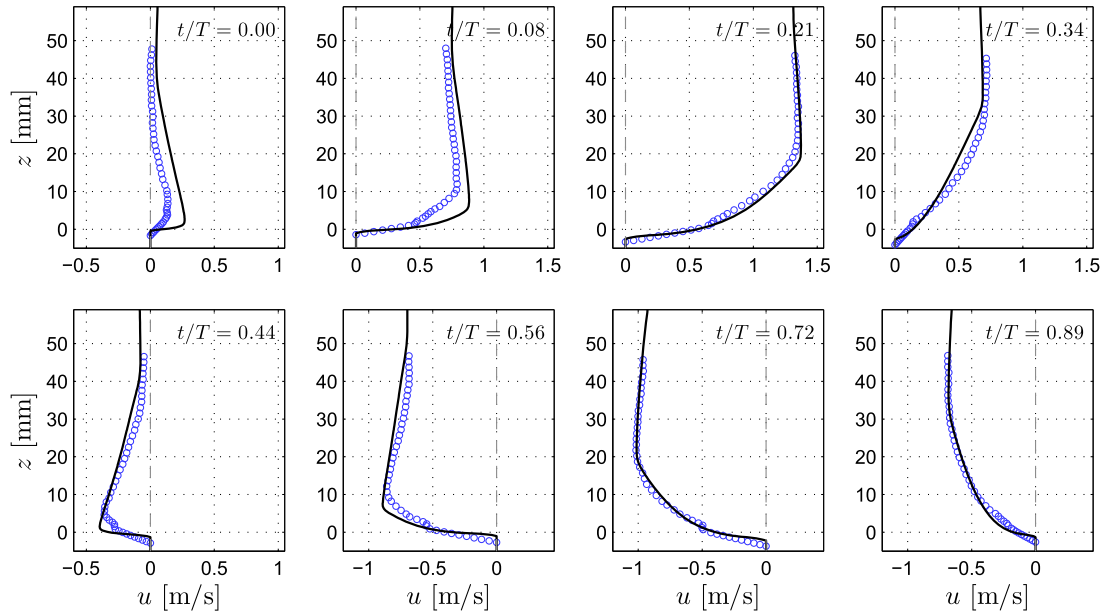


Fig. 6. Comparison of measured (circles) and computed (line) horizontal sediment velocities at various phases of the flow for condition FA7515.

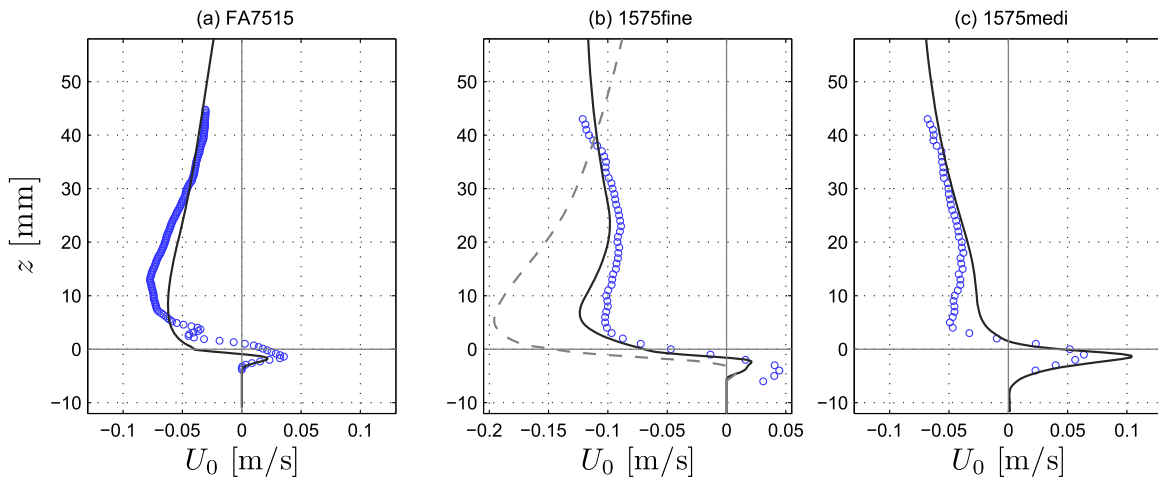


Fig. 7. Comparison of measured (circles) and computed (lines) wave-averaged horizontal velocity U_0 for condition FA7515 (tunnel), 1575fine and 1575medi (both flume). Dashed line in panel b: simulation in tunnel mode, i.e. with progressive wave effects switched off.

includes the boundary layer thickness, the phase lead of the near bed flow, the wave shape streaming and the progressive wave streaming. It also includes the erosion depth asymmetry and the connected onshore current in the bottom part of the sheet-flow layer (the pick-up layer). Also the tilting behavior of the concentration profile (decreasing concentrations beneath and increasing concentrations above the original still bed level during wave phases with increasing (absolute) flow velocities) is reproduced. With this feature, the model shows typical sheet-flow layer behavior. Nevertheless, model-data differences are observed in the shape of some concentration and velocity profiles around flow reversal, possibly indicating room for further improvement of the turbulence model.

5.4. Sensitivity tests

We conclude the validation with a sensitivity analysis. The earlier model adaptation focused on the parameter α . Here we study $C_{\epsilon 3}$, σ_c , β and n , which all potentially influence erosion, turbulence

and the stirring-settling balance and appear in the grain-turbulence interaction terms in Eqs. (10) and (11). The results are shown in Fig. 8, which presents for each test a time series of erosion depth δ_e , a vertical profile of sediment concentration ϕ during maximum onshore flow ($t/T = 0.21$) and a vertical profile of fluid velocity u just after off- to onshore flow reversal ($t/T = 0.0$). All tests simulate condition FA7515 of set ODO. The results for δ_e show that the erosion during maximum on- and offshore flow increases with increasing $C_{\epsilon 3}$ and σ_c . We explain this behavior as follows: an increasing σ_c leads to a decreasing reduction of k from the buoyancy term, Eq. (10), term 4. An increasing $C_{\epsilon 3}$ leads to increasing reduction of ϵ and thus a decreasing dissipation rate of k . For both changes, the larger turbulent kinetic energy induces increased bed shear stresses, leading to larger erosion depths. Obviously, $C_{\epsilon 3}$ is much more influential than σ_c , consistent with the expected dominance of drag effects over buoyancy effects in the concentrated region near the bed. Drag parameter β is present in various parts of the model description, but the tests show that the effect of a reduced/increased β on maximum erosion is very small. The same

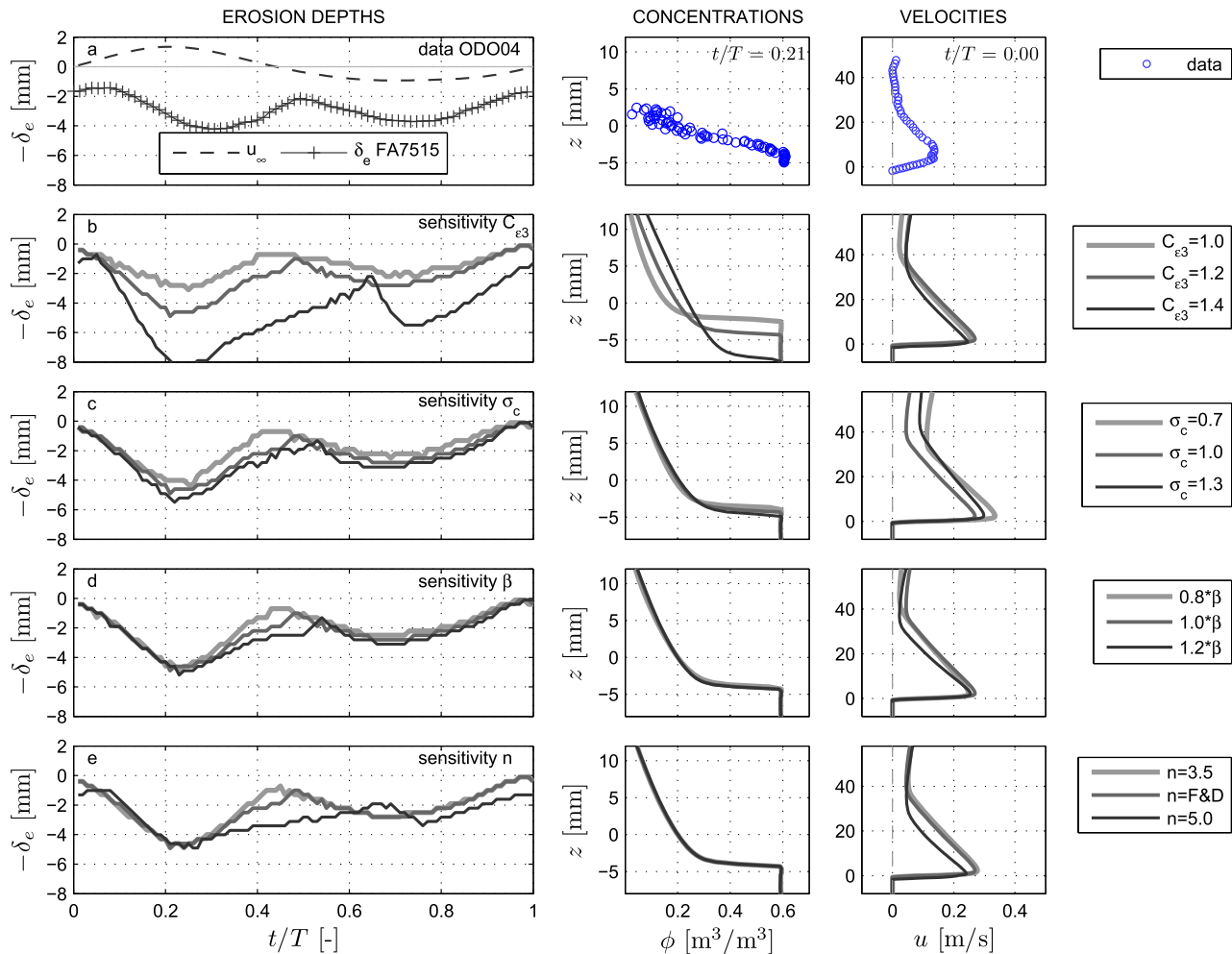


Fig. 8. Sensitivity tests for coefficients in the grain-carrier flow turbulence interaction terms. Column (1) time varying erosion depth δ_e ; column (2) concentration profile at $t/T = 0.21$, maximum onshore flow; column (3) velocity profile at $t/T = 0.02$, just after offshore to onshore flow reversal. Row (a) data condition FA7515 of set ODO; row b–e respectively sensitivity tests for coefficients $C_{\epsilon 3}$, σ_c , β and n . Reference simulation: $C_{\epsilon 3} = 1.2$, $\sigma_c = 1.0$, $\beta = 1.0 \cdot \beta$ from Eq. (6), n following [17]. These tests use the α -function from Eq. (17), with $B = 0.15$.

applies for n that affects the model through the drag coefficient β . In both cases, the dominant effect seems to be the reduction of the settling velocity, which causes a slower return of the bed level towards the initial still bed level and will result in increased phase lag effects. The main conclusions from the sensitivity tests are that the maximum erosion depth δ_e is relatively sensitive for changes in $C_{\epsilon 3}$ and that the return speed of the bed level to the initial still bed level is affected by n and to a smaller degree by β . However, except for $C_{\epsilon 3}$, changes in these parameters do not really affect the shape of the investigated concentration and velocity profiles.

6. Sediment fluxes for fine and medium sized sand in tunnel and flume

Next, we apply the model to investigate trends in sediment flux profiles under influence of grain size variation and progressive wave effects. Hereto, we compare the sediment flux profiles computed for condition MA7515 and FA7515 of the oscillating flow experiments of set ODO with simulations for these same conditions, but now including the effects of the horizontally non-uniform flow field under progressive waves. This is realized by including again the advective terms in the fluid and sediment momentum equations and fluctuation energy equations. Here by, we adopt $c = 5.6$ m/s, belonging to a wave with $T = 7.5$ s in 3.5 m water depth.

Fig. 9 shows profiles of the instantaneous sediment flux both during maximum onshore flow (a and d) and maximum offshore flow (b and e), together with profiles of wave-averaged sediment fluxes (c and f). The first row shows results for medium sized sand, the second row for fine sized sand. Each panel contains flux results obtained from an oscillating flow simulation, a progressive wave simulation and the flow tunnel experiments.

Firstly, note that the oscillatory flow simulations produce instantaneous and period-averaged sediment flux profiles with an order of magnitude and profile shape comparable to the results of the tunnel experiments. This is the case both for the medium and fine sized sand cases. The period averaged results for fine sand are slightly shifted in onshore direction compared to the data, which is directly connected to the earlier observation that for the fine sand condition the erosion depth asymmetry in the model results is larger than in the data. For medium sized sand, the wave averaged flux is underestimated in the lowest part of the profile, resulting from model underestimation of the erosion depth asymmetry in this case. Comparison between the results for oscillatory flow and progressive waves over medium sized sand beds (row 1) shows that the differences in the instantaneous profiles are only small. The period-averaged differences are relatively larger, showing an increased onshore sediment transport rate under progressive waves. For fine sand, we find increased onshore sediment fluxes from progressive waves during maximum onshore flow

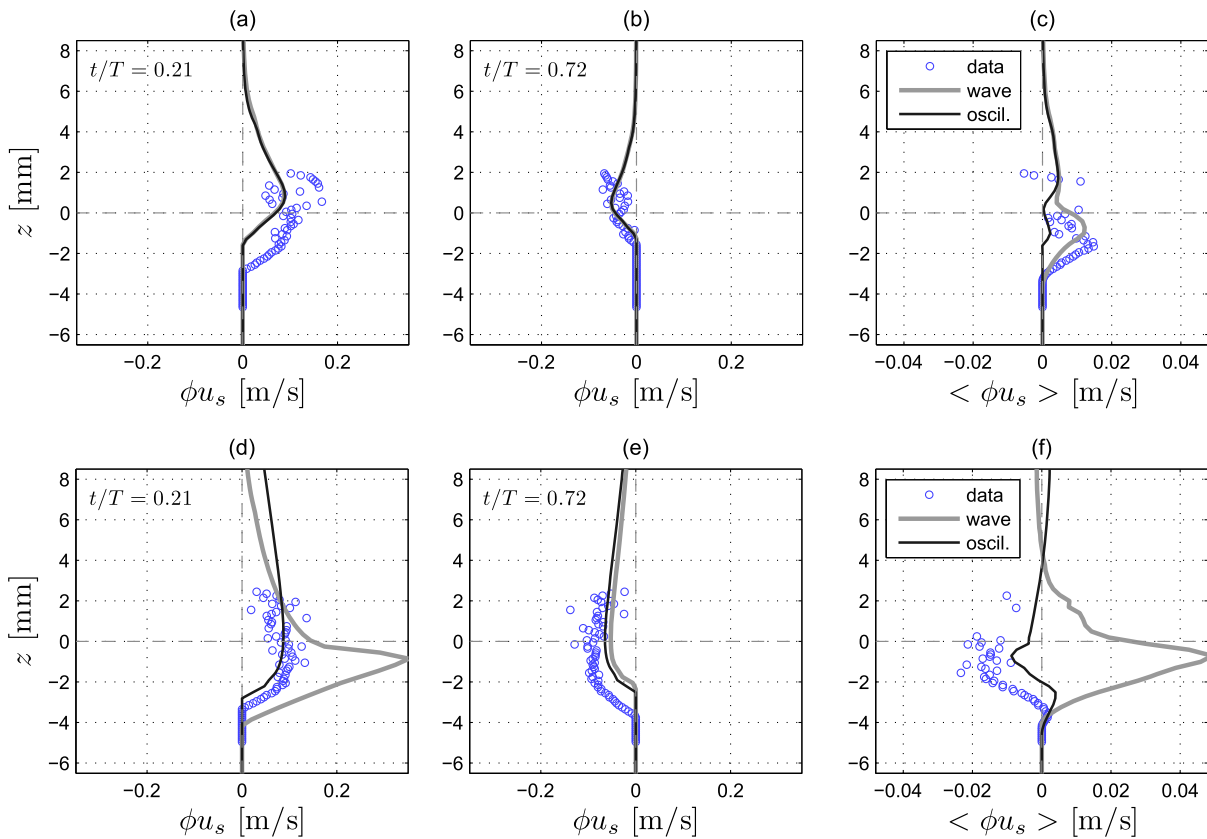


Fig. 9. Vertical profiles of the horizontal sediment flux ϕ_{u_s} . (a and d) during maximum onshore flow; (b and e) during maximum offshore flow; (c and f) period averaged. Upper row: for medium sized sand condition MA7515; lower row: for fine sized sand condition FA7515. Circles: oscillatory flow tunnel experiment; black line: oscillatory flow simulation; gray line: progressive wave simulation.

(panel d), especially in the lower part of the profile. Also the period averaged sediment flux is much larger and clearly onshore directed (f), where the integrated flux in oscillatory flow data and simulation was negative/offshore. Finally, this oscillatory flow – progressive wave difference for fine sand is considerably more significant compared to the difference for medium sized sand (values: medium sized sand: $19 \times 10^{-6} \rightarrow 57 \times 10^{-6} \text{ m}^2/\text{s}$; fine sand: $-20 \times 10^{-6} \rightarrow 127 \times 10^{-6} \text{ m}^2/\text{s}$). The observations from the model results confirm the trend observed by Schretlen [49] for increased onshore transport rates in flume experiments compared to tunnel experiments.

In Fig. 10, the period-averaged sediment flux $\langle \phi_{u_s} \rangle$ is divided in a current related and wave related component, respectively $\langle \phi \rangle \langle u_s \rangle$ and $\langle \tilde{\phi} \tilde{u}_s \rangle$ to study the background of the found differences. Clearly, the most important difference appears in the current-related contribution to the fine sand sediment flux (right panel). However, for fine sand, also the wave-related contribution is affected. Note that below the initial still bed level in general the current-related flux is onshore directed, which is a result of the erosion depth asymmetry under velocity skewed waves/oscillations.

7. Discussion

The results of this study, especially Section 6, provide valuable insights in the behavior of the sheet-flow layer due to grain size variation and progressive wave effects. For sediment transport prediction within morphodynamic modeling systems, it will be very useful to further quantify and parameterize the wave-induced erosion depths and sediment fluxes, including the distribution of

the horizontal flux over the vertical profile. Our study shows that this two-phase model can become an instrument to do this, especially when the behavior around flow reversal could be improved further. What possibilities are present for further improvement and what potential limitations do exist for application in our domain of interest?

Concerning the model formulations, it should be noted that the particle stress closure model has been formulated originally for coarse grains [32]. It is a question whether this closure from collisional theory is still valid in our domain of interest. On the other hand, the importance of this part of the model formulations decreases with decreasing grain size and it was recently shown by Amoudry [2] for medium sized grains and moderate flow that these stress closures could be exchanged with alternative formulations without noteworthy effect on the results.

Considering the turbulence closure, note that the terms to account for particle influence have actually been introduced for very small particles in dilute suspensions. Larger particles could in principle result not only in turbulence damping but also turbulence production, which might invoke the need to add other terms or to adapt the coefficients (Table 1, row 2) of the standard turbulence model terms. However, this is not relevant in the domain of our interest. Nevertheless, indications exist that the Stokes number does not suffice to capture the drag-effect on turbulence and alternative time scale ratios are proposed (e.g. [51]) and could be considered in the future. Simultaneously, there are more fundamental questions concerning the validity of any $k-\epsilon$ -model in the high-concentration region and inside the bed, where the flow might become laminar, and around flow reversal in rather high frequent and vehement oscillations, where a temporary strong reduction of $k-\epsilon$ turbulence production term occurs. With our

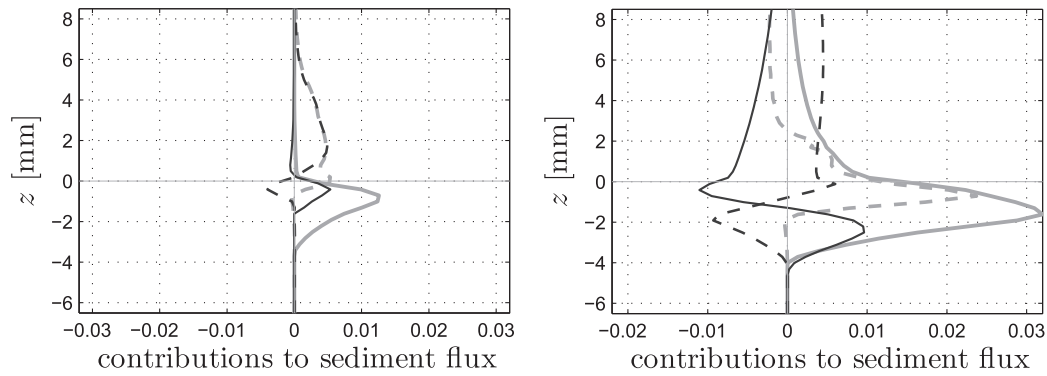


Fig. 10. Current related (continuous line) and wave related (dashed line) contribution to the period averaged sediment flux $\langle \phi u_s \rangle$. Black: oscillatory flow simulations; Gray: progressive wave simulations. (Left) for medium sized sand condition MA7515; (right) for fine sized sand condition FA7515.

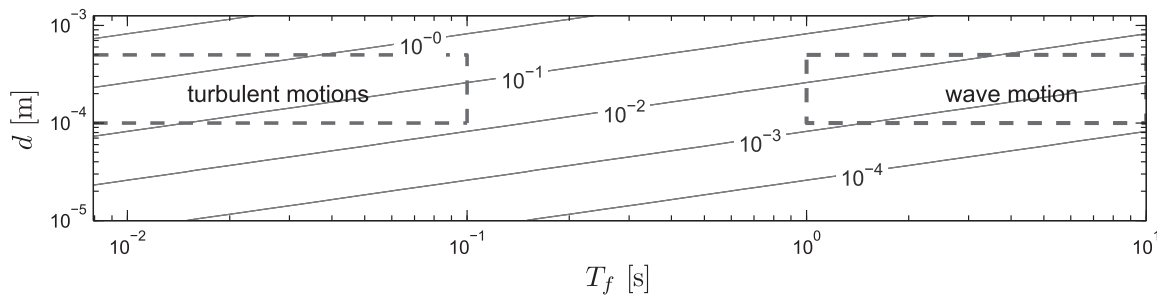


Fig. 11. Contourplot of time-scale ratio T_p/T_f for density ratio $\rho_s/\rho_f = 2.65$ as function of the fluid time scale T_f and the grain size d . For grain sizes of our interest (fine to coarse sand, $0.1 < d < 0.5$ mm), the time scale ratio is about unity for turbulent motions.

application, we might be pushing the k - ε -model beyond its limits: features of shear instabilities [7,23] and short and sudden concentration peaks around flow reversal [42] have been observed in wave boundary layer experiments. These feature can in principle not be captured by the k - ε -turbulence model, and their importance may increase with decreasing grain size (see also [41], who predicted the turbulence generation during flow reversal using a turbulence-resolving model, and [19], who modeled the concentration peak with an adaptation to the original k - ω model of [53]). Although the shear instabilities themselves will not be reproduced by the k - ω model either, some authors suggest that a k - ω closure is better able to deal with the strong shear and turbulence transitions in oscillatory flows (see e.g. [8,19]). Therefore implementation of a k - ω equivalent of Eqs. (10) and (11) might be an interesting next step in modeling sheet-flow beneath waves within the concept of a turbulence-averaged continuous two-phase model.

8. Conclusion

In this study, we predicted erosion depths and sediment fluxes, and their dependency on grain size and streaming with an Eulerian two-phase model. Our first conclusion is that the model results for erosion are very sensitive to the modeling of the grain influence on fluid turbulence. With a new grain induced turbulence damping function proposed in this study, we extend the applicability of the model towards finer grain sizes and obtain a correct grain size dependent behavior and good reproduction of measured erosion depths of coarse, medium and fine sized sand beds.

We conclude from model-data comparison on concentration and velocity profiles that the model is able to reproduce a number of important sheet-flow and boundary layer characteristics. This includes the tilting motion of the concentration profile during the wave, which is important, because this behavior reflects the

typical structure of the sheet-flow layer, with respectively a pick-up layer with decreasing concentrations and an upper sheet-flow layer with increasing concentrations under increasing (absolute) flow velocities. As a result, the model is able to produce fluxes over the entire sheet-flow layer, also below the original bed level. Next, the model reproduces the phase lead of the near-bed flow over the free stream and the maximum thickness of the boundary layer. We also find the experimentally observed positive streaming inside the sheet-flow layer, the negative current at slightly higher levels – both resulting from velocity-skewness – and the progressive wave effect on the streaming profile. The model reproduction of the first feature is an important improvement over earlier streaming profile predictions with single-phase models.

In a model investigation on trends in sediment flux profiles under influence of grain size variation and progressive wave effects, we found period-averaged sediment fluxes increasingly onshore directed under influence of wave progression, both for medium and fine sand. The effect is most drastic for fine sand. We conclude from decomposition of the period-averaged sediment flux profile in a current-related and wave-related contribution, that the major part of the increased onshore transport of fine sand can be attributed to the current-related contribution. This underlines the need to account for progressive wave streaming in numerical models and sediment transport formulas. Finally, we conclude that the present two-phase model is a valuable instrument for further study and parameterization of sheet-flow layer processes.

Acknowledgements

We thankfully acknowledge Dr. X. Yu, University of Delaware, Newark, DE, US, for sharing his code and Dr. J.L.M. Schretlen, University of Twente, Enschede, NL, for providing data. Also the financial support of the internal fund of the University of Delaware for visiting the Center for Applied Coastal Research (CACR) and

funding from the Joint Research Activity WISE within the EU-project HYDRALAB-IV, and the joint STW/EPSC project SINBAD is gratefully acknowledged.

Appendix A. Drag-related terms in the turbulence model

A.1. Grain–fluid turbulence interaction terms

The influence of the drag force on the ensemble-averaged energy of the fluid fluctuations appears in the equation for turbulent kinetic energy as:

$$DRAG_k = -\beta \left[\overline{\phi \Delta u^f} (\tilde{u}^f - \tilde{u}^s) + \overline{\phi \Delta u^f (\Delta u^f - \Delta u^s)} \right] \quad (18)$$

Hereby the overbar denotes ensemble-averaging, while \tilde{u} and Δu denote respectively the (Favre-)ensemble-averaged and fluctuating velocity vector of either fluid (^f) or sediment (^s). The first term is modeled using the gradient transport assumption. Hereby, the contribution of the horizontal concentration gradient and slip velocity is neglected compared to the vertical. Next, equilibrium is assumed between vertical drag and gravity, which transforms this drag contribution to a buoyancy term as appears in Eqs. (10) and (11), fourth term.

$$-\beta \overline{\phi \Delta u^f} (\tilde{u}^f - \tilde{u}^s) \approx \beta \frac{v_{ft}}{\sigma_c} \frac{\partial \bar{\phi}}{\partial z} (\tilde{w}^f - \tilde{w}^s) \approx (\rho_s - \rho_f) g \frac{v_{ft}}{\sigma_c} \frac{\partial \bar{\phi}}{\partial z} \quad (19)$$

In modeling the second term, the triple correlation between concentration and velocity fluctuations is neglected (compare [11]), and the correlation $\overline{\Delta u^f \Delta u^s}$ is expressed in the correlation $\overline{\Delta u^f \Delta u^f} \approx 2k$ through parameter α . This yields:

$$\begin{aligned} -\beta \overline{\phi \Delta u^f (\Delta u^f - \Delta u^s)} &\approx -\beta \overline{\phi \Delta u^f (\Delta u^f - \Delta u^s)} \\ &= -\beta \bar{\phi} (1 - \alpha) \overline{\Delta u^f \Delta u^f} \approx -2\beta \bar{\phi} (1 - \alpha) k \end{aligned} \quad (20)$$

appearing in Eqs. (10) and (11), fifth term.

A.2. Derivation of α -functions

The next step is to find an expression for α . Assuming for the turbulent/fluctuating motion of fluid and sediment (considering one direction):

$$\Delta u^f = \text{Re}(\widehat{\Delta u^f} e^{i\omega t}); \quad \Delta u^s = \text{Re}(\eta e^{i\varphi} \widehat{\Delta u^f} e^{i\omega t}) \quad (21)$$

with η the amplitude ratio and φ a phase difference between grain and fluid motion, the ratio of the ensemble averaged correlations becomes $\alpha = \overline{\Delta u^f \Delta u^s} / \overline{\Delta u^f \Delta u^f} = \eta \cos(\varphi)$.

Expressions for η and φ can then be derived from transfer functions. These functions result from the coupled momentum equations of fluid and sediment, see [24,25]. The formulation of these momentum equations is of course depending on the forces taken into account. For a volume, partly filled with fluid and partly with sediment, that accelerates under influence of a pressure gradient and where fluid and sediment interact through drag, the momentum equations read:

$$(1 - \phi) \rho_f \frac{du_f}{dt} = -(1 - \phi) \frac{dP}{dx} - \phi \beta (u_f - u_s) \quad (22)$$

$$\phi \rho_s \frac{du_s}{dt} = -\phi \frac{dP}{dx} + \phi \beta (u_f - u_s) \quad (23)$$

which after substitution can be written as:

$$\frac{du_s}{dt} + au_s = b \frac{du_f}{dt} + au_f; \quad \text{with } a = \left(1 + \frac{\phi}{(1 - \phi)}\right) \frac{\beta}{\rho_s}; \quad b = \frac{\rho_f}{\rho_s} \quad (24)$$

Alternatively, when neglecting feedback of sediment on the flow in case of small concentrations ($\phi \rightarrow 0$), a becomes $a = \beta / \rho_s = 1/T_p$. Considering only acceleration of the sediment through drag between sediment and a fluid moving with a given velocity, $b = 0$. (Likewise, the coefficients will change when accounting for additional forces not considered here, like the added mass force, see [25]).

Considering fluid and sediment motion as a summation of Fourier components with angular frequency ω and defining for each component $u_f = \hat{u}_f e^{i\omega t}$ and $u_s = \eta e^{i\varphi} \hat{u}_f e^{i\omega t}$, it follows from Eq. (24) that for each component:

$$\eta e^{i\varphi} = \frac{i\omega b + a}{i\omega + a} \quad (25)$$

From this, η and φ can be computed:

$$\eta = \sqrt{\text{Re}^2(A) + \text{Im}^2(A)}; \quad \varphi = \text{atan}\{\text{Im}(A)/\text{Re}(A)\} \quad (26)$$

with A the RHS of Eq. (25). Multiplication of nominator and denominator with $(i\omega - a)/a^2$ yields distinct real and imaginary parts and an expression for α :

$$\eta e^{i\varphi} = \frac{\omega^2 b + 1}{\omega^2 + 1} + i \frac{\omega(b - 1)}{\omega^2 + 1}; \quad (27)$$

$$\alpha = \eta \cos(\varphi) = \text{Re}\{\eta e^{i\varphi}\} = \frac{1 + \frac{\omega^2 b}{a^2}}{1 + \frac{\omega^2}{a^2}}$$

where the α coupled to the (time and location dependent) typical turbulent time-scale $T_t = 1/6 k_f/\epsilon_f$ through $\omega = 2\pi/T_t$ is the one used in the calculations.

When we consider only sediment acceleration by drag, $a = \beta/\rho_s = 1/T_p$ and $b = 0$, and α reads:

$$\alpha = \frac{1}{1 + (2\pi)^2 \left(\frac{T_p}{T_t}\right)^2} \quad (28)$$

This provides the basis for the newly proposed α -function of Eq. (14). Considering that also factors other than 1/6 are found in literature to relate the fluid time-scale to the turbulence parameters, we allow c_1 of Eq. (14) to be used as tuning parameter. Also the more complicated expressions for α resulting from Eq. (27) with the alternative values of a and b have been studied. This yielded no further improvement and is therefore not elaborated here.

Finally, an estimation of the time scale ratio through our domain of interest is given in Fig. 11. For simplicity, the particle time scale is estimated from the viscous drag only, which yields:

$$\frac{T_p}{T_f} = \frac{\rho_s}{\beta} \frac{1}{T_f} = \frac{1}{2\pi} \frac{1}{18} \frac{\rho_s}{\rho_f} \frac{d^2 \omega}{v} \quad (29)$$

Eq. (28) shows that relevant changes in α occur for $10^{-1} < T_p/T_f < 10^1$. So the figure indicates that fluid–grain velocity differences may be expected for the turbulent motions and thus that drag will become relevant for the turbulence model.

References

- [1] Ahilan RV, Sleath JFA. Sediment transport in oscillatory flow over flat beds. J Hydraul Eng 1987;113(3):308–22. [http://dx.doi.org/10.1061/\(ASCE\)0733-9429\(1987\)113:3\(308\)](http://dx.doi.org/10.1061/(ASCE)0733-9429(1987)113:3(308)).
- [2] Amoudry LO. Assessing sediment stress closures in two-phase sheet flow models. Adv Water Resour 2012;48:92–101. <http://dx.doi.org/10.1016/j.advwatres.2012.03.011>.

- [3] Amoudry L, Hsu T-J, Liu PL-F. Two-phase model for sand transport in sheet flow regime. *J Geophys Res* 2008;113(C3):1–15. <http://dx.doi.org/10.1029/2007JC004179>.
- [4] Asano T. Two-phase flow model on oscillatory sheet flow. In: Proceedings of 22th international conference on coastal engineering, New York, US: ASCE; 1990. p. 2372–84. <<http://journals.tdl.org/icce/index.php/icce/article/view/4608>>.
- [5] Bagnold RA. Experiments on a gravity-free dispersion of large solid spheres in a Newtonian fluid under shear. *Proc R Soc A: Math Phys Eng Sci* 1954;225(1160):49–63. <http://dx.doi.org/10.1098/rspa.1954.0186>.
- [6] Blondeaux P, Vittori G, Bruschi A, Lalli F, Pesarino V. Steady streaming and sediment transport at the bottom of sea waves. *J Fluid Mech* 2012;697:115–49. <http://dx.doi.org/10.1017/jfm.2012.50>.
- [7] Carstensen S, Sumer BM, Fredsøe J. Coherent structures in wave boundary layers. Part 1. Oscillatory motion. *J Fluid Mech* 2010;646:169. <http://dx.doi.org/10.1017/S0022112009992825>.
- [8] Cavallaro L, Scandura P, Foti E. Turbulence-induced steady streaming in an oscillating boundary layer: on the reliability of turbulence closure models. *Coastal Eng* 2011;58(4):290–304. <http://dx.doi.org/10.1016/j.coastaleng.2010.10.001>.
- [9] Chen CP, Wood PE. A turbulence closure model for dilute gas-particle flows. *Can. J. Chem. Eng.* 1985;63(3):349–60. <http://dx.doi.org/10.1002/cice.5450630301>.
- [10] Conley DC, Falchetti S, Lohmann IP, Brocchini M. The effects of flow stratification by non-cohesive sediment on transport in high-energy wave-driven flows. *J Fluid Mech* 2008;610:43–67. <http://dx.doi.org/10.1017/S0022112008002565>.
- [11] Danon H, Wolfshtein M, Hetsroni G. Numerical calculations of two-phase turbulent round jet. *Int J Multiphase Flow* 1977;3(1960):223–34. [http://dx.doi.org/10.1016/0301-9322\(77\)90002-7](http://dx.doi.org/10.1016/0301-9322(77)90002-7).
- [12] Dohmen-Janssen CM, Kroekenstoel DF, Hassan WN, Ribberink JS. Phase lags in oscillatory sheet flow: experiments and bed load modelling. *Coastal Eng* 2002;46(1):61–87. [http://dx.doi.org/10.1016/S0378-3839\(02\)00056-X](http://dx.doi.org/10.1016/S0378-3839(02)00056-X).
- [13] Dohmen-Janssen CM, Hanes DM. Sheet flow dynamics under monochromatic nonbreaking waves. *J Geophys Res* 2002;107(C10):1–21. <http://dx.doi.org/10.1029/2001JC001045>.
- [14] Dong P, Zhang K. Two-phase flow modelling of sediment motions in oscillatory shear. *Coastal Eng* 1999;36(2):87–109. [http://dx.doi.org/10.1016/S0378-3839\(98\)00052-0](http://dx.doi.org/10.1016/S0378-3839(98)00052-0).
- [15] Drew DA. Production and dissipation of energy in the turbulent flow of a particle–fluid mixture, with some results on drag reduction. *J Appl Mech* 1976;43(4):543–7. <http://dx.doi.org/10.1115/1.3423926>.
- [16] Elghobashi SE, Abou-Arab TW. A two-equation turbulence model for two-phase flows. *Phys Fluids* 1983;26(4):931. <http://dx.doi.org/10.1063/1.864243>.
- [17] Fredsøe J, Deigaard R. Mechanics of coastal sediment transport, world scientific. *Adv Series Ocean Eng.* vol. 3. 1992.
- [18] Fuhrman DR, Schløer S, Sterner J. RANS-based simulation of turbulent wave boundary layer and sheet-flow sediment transport processes. *Coastal Eng* 2013;73:151–66. <http://dx.doi.org/10.1016/j.coastaleng.2012.11.001>.
- [19] Guizien K, Dohmen-Janssen CM, Vittori G. 1DV bottom boundary layer modeling under combined wave and current: turbulent separation and phase lag effects. *J Geophys Res* 2003;108(C1):1–15. <http://dx.doi.org/10.1029/2001JC001292>.
- [20] Hanes DM, Inman DL. Observations of rapidly flowing granular–fluid materials. *J Fluid Mech* 1985;150:357–80. <http://dx.doi.org/10.1017/S0022112085000167>.
- [21] Hassan WNM, Ribberink JS. Modelling of sand transport under wave-generated sheet flows with a RANS diffusion model. *Coastal Eng* 2010;57(1):19–29. <http://dx.doi.org/10.1016/j.coastaleng.2009.08.009>.
- [22] Henderson SM, Allen JS, Newberger PA. Nearshore sandbar migration predicted by an eddy-diffusive boundary layer model. *J Geophys Res* 2004;109(C6):1–15. <http://dx.doi.org/10.1029/2003JC002137>.
- [23] Henriquez M, Reniers AJHM, Ruessink BG, Stive MJF. Vortex tubes in the wave bottom boundary layer. In: Kranenburg WM, Horstman EM, Wijnberg KM, editors. NCK-days 2012: jubilee conference proceedings 20th NCK-days, University of Twente: Enschede, The Netherlands; 2012. p. 143–146. <http://dx.doi.org/10.3990/2.185>.
- [24] Hinze JO. Turbulence. In: Clark BJ, editor. McGraw-Hill series in mechanical engineering, 2nd ed. 1975.
- [25] Hjelmfelt AT, Mockros LF. Motion of discrete particles in a turbulent fluid. *Appl Sci Res* 1966;16:149–61. <http://dx.doi.org/10.1007/BF00384062>.
- [26] Holmedal LE, Myrhaug D. Boundary layer flow and net sediment transport beneath asymmetrical waves. *Cont Shelf Res* 2006;26(2):252–68. <http://dx.doi.org/10.1016/j.csr.2005.11.004>.
- [27] Holmedal LE, Myrhaug D. Wave-induced steady streaming, mass transport and net sediment transport in rough turbulent ocean bottom boundary layers. *Cont Shelf Res* 2009;29(7):911–26. <http://dx.doi.org/10.1016/j.csr.2009.01.012>.
- [28] Hsu T-J, Elgar S, Guza RT. Wave-induced sediment transport and onshore sandbar migration. *Coastal Eng* 2006;53(10):817–24. <http://dx.doi.org/10.1016/j.coastaleng.2006.04.003>.
- [29] Hsu T-J, Jenkins JT, Liu PL-F. On two-phase sediment transport: dilute flow. *J Geophys Res* 2003;108(C3). <http://dx.doi.org/10.1029/2001JC001276>.
- [30] Hsu T-J, Jenkins JT, Liu PL-F. On two-phase sediment transport: sheet flow of massive particles. *Proc R Soc A: Math Phys Eng Sci* 2004;460(2048):2223–50. <http://dx.doi.org/10.1098/rspa.2003.1273>.
- [31] Hsu T-J, Hanes DM. Effects of wave shape on sheet flow sediment transport. *J Geophys Res* 2004;109(C5):1–15. <http://dx.doi.org/10.1029/2003JC002075>.
- [32] Jenkins JT, Hanes DM. Collisional sheet flows of sediment driven by a turbulent fluid. *J Fluid Mech* 1998;370:29–52. <http://dx.doi.org/10.1017/S0022112098001840>.
- [33] Jenkins JT, Savage SB. A theory for the rapid flow of identical, smooth, nearly elastic particles. *J Fluid Mech* 1983;130:187–202. <http://dx.doi.org/10.1017/S0022112083001044>.
- [34] Kranenburg WM. Modeling sheet-flow sand transport under progressive surface waves [PhD Thesis]. University of Twente: Enschede, The Netherlands; 2013. <http://dx.doi.org/10.3990/1.9789036535045>.
- [35] Kranenburg WM, Ribberink JS, Schretlen JLM, Uittenbogaard RE. Sand transport beneath waves: the role of progressive wave streaming and other free surface effects. *J Geophys Res: Earth Surface* 2013;118. <http://dx.doi.org/10.1029/2012JF002427>.
- [36] Kranenburg WM, Ribberink JS, Uittenbogaard RE, Hulscher SJMH. Net currents in the wave bottom boundary layer: on wave shape streaming and progressive wave streaming. *J Geophys Res* 2012;117(F03005). <http://dx.doi.org/10.1029/2011JF002070>.
- [37] Li M, Pan S, O'Connor BA. A two-phase numerical model for sediment transport prediction under oscillatory sheet flows. *Coastal Eng* 2008;55(12):1159–73. <http://dx.doi.org/10.1016/j.coastaleng.2008.05.003>.
- [38] Longuet-Higgins MS. The mechanics of the boundary-layer near the bottom in a progressive wave. In: Proceedings of 6th conference on coastal engineering, Berkeley, USA: ASCE; 1958. p. 184–193.
- [39] Marchioli C, Picciotto M, Soldati A. Particle dispersion and wall-dependent turbulent flow scales: implications for local equilibrium models. *J Turbul* 2006;7(60). <http://dx.doi.org/10.1080/14685240600925171>.
- [40] McTigue DF. Mixture theory for suspended sediment transport. *J Hydraul Div ASCE* 1981;107(6):659–73. <<http://cedb.asce.org/cgi/WWWdisplay.cgi?10264>>.
- [41] Ozdemir CE, Hsu T-J, Balachandrar S. A numerical investigation of fine particle laden flow in an oscillatory channel: the role of particle-induced density stratification. *J Fluid Mech* 2010;665(2010):1–45. <http://dx.doi.org/10.1017/S0022112010003769>.
- [42] O'Donoghue T, Wright S. Concentrations in oscillatory sheet flow for well sorted and graded sands. *Coastal Eng* 2004;50(3):117–38. <http://dx.doi.org/10.1016/j.coastaleng.2003.09.004>.
- [43] O'Donoghue T, Wright S. Flow tunnel measurements of velocities and sand flux in oscillatory sheet flow for well-sorted and graded sands. *Coastal Eng* 2004;51(11–12):1163–84. <http://dx.doi.org/10.1016/j.coastaleng.2004.08.001>.
- [44] Richardson JF, Zaki WN. Sedimentation and fluidisation: Part I. *Trans Inst Chem Eng* 1954;32:S82–S100. [http://dx.doi.org/10.1016/S0263-8762\(97\)80006-8](http://dx.doi.org/10.1016/S0263-8762(97)80006-8).
- [45] Van Rijn LC, Tonnon PK, Walstra DJR. Numerical modelling of erosion and accretion of plane sloping beaches at different scales. *Coastal Eng* 2011;58(7):637–55. <http://dx.doi.org/10.1016/j.coastaleng.2011.01.009>.
- [46] Rodi W. Examples of calculation methods for flow and mixing in stratified flows. *J Geophys Res* 1987;92(C5):5305–28. <http://dx.doi.org/10.1029/JC092iC05p05305>.
- [47] Ruessink BG, van den Berg TJJ, van Rijn LC. Modeling sediment transport beneath skewed asymmetric waves above a plane bed. *J Geophys Res* 2009;114(C11):1–14. <http://dx.doi.org/10.1029/2009JC005416>.
- [48] Rundqvist R, Ljus C, van Wachem B. Experimental and numerical investigation of particle transport in a horizontal pipe. *AIChE J* 2005;51(12):3101–8. <http://dx.doi.org/10.1002/aic.10571>.
- [49] Schretlen JLM. Sand transport under full-scale progressive surface waves [PhD-thesis]. Enschede, The Netherlands: University of Twente; 2012. <<http://purl.utwente.nl/publications/80884>>
- [50] Squires KD, Eaton JK. Effect of selective modification of turbulence on two-equation models for particle-laden turbulent flows. *J Fluids Eng* 1994;116(4):778. <http://dx.doi.org/10.1115/1.2911849>.
- [51] Toorman EA. Vertical mixing in the fully developed turbulent layer of sediment-laden open-channel flow. *J Hydraul Eng* 2009;134(9):1225–35. [http://dx.doi.org/10.1061/\(ASCE\)10733-9429\(2008\)134:9\(1225\)](http://dx.doi.org/10.1061/(ASCE)10733-9429(2008)134:9(1225)).
- [52] Trowbridge J, Madsen OS. Turbulent wave boundary layers 2. Second-order theory and mass transport. *J Geophys Res* 1984;89(C5):7999–8007. <http://dx.doi.org/10.1029/JC089iC05p07999>.
- [53] Wilcox DC. Turbulence modeling in CFD. 1st ed. Ind., Inc., La Canada, Calif; 1994.
- [54] Yu X, Hsu T-J, Jenkins JT, Liu PL-F. Predictions of vertical sediment flux in oscillatory flows using a two-phase, sheet-flow model. *Adv Water Resour* 2012;48:2–17. <http://dx.doi.org/10.1016/j.advwatres.2012.05.012>.
- [55] Yu X, Hsu T-J, Hanes DM. Sediment transport under wave groups: relative importance between nonlinear washphase and nonlinear boundary layer streaming. *J Geophys Res* 2010;115(C2):1–18. <http://dx.doi.org/10.1029/2009JC005348>.
- [56] Zhang Y, Campbell CS. The interface between fluid-like and solid-like behaviour in two-dimensional granular flows. *J Fluid Mech* 1992;237:541–68. <http://dx.doi.org/10.1017/S0022112092003525>.
- [57] Swart DH. Offshore sediment transport and equilibrium beach profiles. Delft, The Netherlands: Delft Hydraulics Laboratory; 1974. Publication no. 131.